Adaptive Bootstrap Design for Hybrid Terrestrial Broadcast and Mobile Communication Networks

Yihang Huang, Dazhi He, *Member, IEEE*, Wenjun Zhang, *Fellow, IEEE*, Yin Xu, and Yunfeng Guan

***Abstract*—The bootstrap in ATSC 3.0 is expected to act as a universal wake-up signal for various wireless systems in addition to broadcast network. However, the signaling decoding performance of the standardized bootstrap degrades significantly in channels of fast time-variation and strong multipath. Furthermore, part of available bandwidth is reserved to ensure the compatibility with mobile communication network (MCN), which puts a limitation on the performance improvement. In this paper, to make the best of the available bandwidth, we introduce the bandwidth-concerned version information to enable an adaptive bandwidth configuration for the proposed bootstrap. Moreover, a 2-D signaling scheme is used to increase signaling capacity by selecting different gold sequences in frequency domain (FD) and simultaneously applying cyclic shift in time domain (TD). At the receiver side, we first provide improved estimators of symbol timing offset (STO) and fine frequency offset (FFO) for the bootstrap with special TD structure. Meanwhile, a learning-based binary classifier taking the output of STO estimator as training data is provided to generate an SNR-independent threshold for spectrum sensing without requiring the knowledge of channel conditions nor noise estimator. Afterwards, an inverse fast Fourier transform (IFFT)-based algorithm is used to decode FD signaling in the presence of unknown TD signaling, which allows 3-bit higher signaling capacity. Numerical analysis and simulation results demonstrate that the proposed adaptive bootstrap design as well as corresponding receiver algorithms significantly outperform the standardized one in terms of synchronization, detection and signaling decoding.**

***Index Terms*—Bootstrap, synchronization, spectrum sensing, signaling transmission, hybrid network.**

I. Introduction

EXPLOSIVE growth of high-speed data applications has led to much more data traffic demand for future wireless network. The next-gen wireless communication network, 5G, has the promise of supporting mass data transmission by improving the spectrum efficiency on one hand, and by extending the available spectrum on the other hand [1], [2]. As for higher spectrum efficiency, the broadcast mode in cellular system, MBMS, is recommended to deliver popular and public video to a large number of subscribers pursuing the same content [3]. However, the MBMS is rarely adopted in practice because of the hard tradeoff among business profit, network flexibility and spectrum efficiency [4]. Meanwhile, the broadcast industry has the vision to cooperate with wireless communication entity on the basis of well-established infrastructures and well-developed technologies. Now 5G-Xcast of 5GPPP Phase II projects is in progress, which focuses on the broadcast and multicast communication enablers for 5G. Large amount of research topics in relation to signal processing, spectrum management and caching strategy are widely investigated [5], [6]. Thereinto, system discovery and synchronization mechanisms are important issues referring to system indication, signal acquisition and spectrum sensing, when physical frames from different systems are time-multiplexed in a broadcast-only mode [7], [8]. The preamble signal is an efficient tool to deal with this issue in low cost because of its high design flexibility and low resource occupation. In hybrid network, a unified preamble signal is required to enable high-efficiency signaling transmission in short period and adapt to various systems in severe environments.

The latest DTTB standards, DVB-T2 and ATSC 3.0, have specified some specially-coded OFDM symbols to enable service discovery and deliver transmission parameter signaling (TPS) at low signal levels. The bootstrap adopted by ATSC 3.0 consists of multiple OFDM symbols, which ensures preferable performance on both synchronization and signaling decoding [9]. Some parameters like sampling rate, bandwidth and FFT size are specially designed for compatibility with mobile communication system. The bootstrap occupies a bandwidth of 4.5MHz, which is smaller than the required bandwidth of cellular system in most cases [10]. The total time duration of the bootstrap, 2ms, is designed to support easy multiplex with cellular frame, which has an integer milliseconds period [11]. However, the time-domain signaling transmission scheme of the standardized bootstrap encounters considerable performance degradation in strong multipath channel as described in [12]. Moreover, only part of the subcarriers in the frequency domain are exploited, so about 1.5MHz bandwidth is wasted during the transmission of the bootstrap signal. Huang *et al.* [12] proposed a FD signaling transmission scheme to eliminate the side peaks introduced by strong multipath. In addition, all subcarriers are exploited to further improve the decoding performance. However, the correlation property of zero correlation zone (ZCZ) sequence utilized

Manuscript received November 1, 2018; revised January 13, 2019; accepted March 24, 2019. This work was supported in part by the National Natural Science Foundation of China under Grant 61601286, Grant 61671297, and Grant 61420106008, in part by the Shanghai Key Laboratory of Digital Media Processing under Grant STCSM18DZ2270700, in part by the National Science and Technology Major Project under Grant 2017ZX03001027, and in part by the Scientific and Innovative Action Plan of Shanghai under Grant 17511106102. *(Corresponding author: Dazhi He.)*

The authors are with the School of Electronic Information and Electrical Engineering, Shanghai Jiao Tong University, Shanghai 200240, China (e-mail: hedazhi@sjtu.edu.cn).

Color versions of one or more of the figures in this paper are available online at http://ieeexplore.ieee.org.

Digital Object Identifier 10.1109/TBC.2019.2909196

in [12] degrades significantly along with the decrease of the sequence length, which indicates poor performance in cellular scenario where bandwidth is limited.

In order to address the issue on tradeoff between signaling transmission performance and multiple systems compatibility, a unified bootstrap design with adaptive bandwidth determined by system type is proposed in this paper. The main contributions of this paper are summarized as below:

- We propose an adaptive bootstrap design with new signaling transmission scheme, which has better signaling decoding performance and higher signaling transmission capacity than the standardized one. We introduce a bandwidth-concerned version signaling into the first bootstrap symbol to inform the receiver of the signal bandwidth and time-frequency two-dimensional (2D) signaling into subsequent bootstrap symbols to achieve higher capacity without performance degradation. We propose to generate the adaptive bootstrap with different bandwidths from the same originating sequence but with different truncating lengths. The combination of a Zadoff-Chu (ZC) sequence and a Gold sequence is adopted as the originating sequence, because its good cross correlation and autocorrelation properties in both complete and truncated status ensure the robust decoding of any signaling by diverse receivers. On this basis, 8-bit FD signaling is encoded by employing different Gold sequences and 3-bit extra TD signaling is carried by TD cyclic shifts simultaneously.
- We propose some related receiver algorithms to further improve the performances from multiple aspects. we firstly derive the log-likelihood function (LLF) of the bootstrap symbol with CAB-BCA structure to provide a footstone for synchronization improvement and then utilize it to preliminarily accomplish time delay and FFO estimation. As for spectrum sensing, support vector machine (SVM) is utilized to generate a SNR-independent threshold in case that the channel condition and noise variance are unknown. With regard to the two-dimensional signaling decoder, IFFT operation is firstly exploited to pick the correct FD sequence in the face of unknown TD cyclic shift brought in by TD signaling, and then TD signaling can be decoded in exactly the same way as the standardized bootstrap.
- Finally, theoretical evaluations and numerical simulations are conducted. We firstly derive the tractable signaling error rate of the proposed 2D signaling scheme in AWGN channel and reveal the relationship between FD and TD signaling. After that, qualitative comparisons between the proposed and standardized bootstrap are made in strong-multipath and fast time-selective fading channels, which indicate a better decoding performance of the proposed one. Numerical simulations are presented to further demonstrate the superior performance of the proposed bootstrap design along with the receiver algorithms.

The rest of the paper is organized as follows. In Section II, the standardized bootstrap in ATSC 3.0 is briefly reviewed. The proposed bootstrap design and corresponding receiver algorithms concerning synchronization, detection and signaling decoding are sequentially presented in Sections III and IV. Section V provides theoretical analyses on both standardized bootstrap and proposed bootstrap. Our simulation results are reported and discussed in Section VI. Finally, conclusions are drawn in Section VII.

II. Overview of the ATSC 3.0 Bootstrap

The standardized bootstrap, originated from a combined sequence between Zadoff-Chu (ZC) sequence Z and pseudo-noise (PN) sequence P, preserves good correlation properties in both time domain and frequency domain. After subcarrier mapping and zero padding, the FD signal of each bootstrap symbol can be represented as

$$S_n(k) = \begin{cases} Z(k+749) \times P((n+1)\cdot 749 + k), & -749 \le k \le -1 \\ Z(k+749) \times P((n+1)\cdot 749 - k), & 1 \le k \le 749 \\ 0, & otherwise \end{cases} \tag{1}$$

Let $\tilde{A}_n$ represent the time domain sequence derived as the 2048-point IFFT of (1), the cyclically shifted sequence with TPS applied can be represented as

$$A_n(t) = \tilde{A}_n((t + M_n) \bmod 2048) \tag{2}$$

where, n is the index of bootstrap symbols, M_n is the absolute cyclic shift obtained by combining a Grey code mapper and an accumulator [9]. Let N_b specify the number of valid signaling bits in each symbol and let $b_0^n, \ldots, b_{N_b-1}^n$ represent the values of those bits. The output of the Grey code mapper can be written as

$$m_i^n = \begin{cases} \left(\sum_{k=0}^{10-i} b_k^n\right) \bmod 2, & i > 10 - N_b \\ 1, & i = 10 - N_b \\ 0, & i < 10 - N_b \end{cases} \tag{3}$$

The decimal representation of the coded signaling bits $m_{10}^n \ldots m_1^n m_0^n$ is defined to be the relative cyclic shift $\tilde{M}_n$. The absolute cyclic shift M_n of (2) can be obtained by iterative accumulation as follows

$$M_n = \begin{cases} 0, & n = 0 \\ \left(M_{n-1} + \tilde{M}_n\right) \bmod 2048, & 1 \le n < 4 \end{cases} \tag{4}$$

There are two variants of the time domain structure with different guard interval insertion as shown in Fig. 1. Part C represents the cyclic prefix with a length of N_C (520) samples, which is directly taken from part A. Part B with a length of N_B (504) samples acts as the frequency shifted postfix or hyper-prefix. The first bootstrap symbol used for sync detection adopts CAB variant and remaining bootstrap symbols carrying system parameters employ BCA variant.

At the receiver side, delayed correlation and local sequence based correlation (LSBC) have been proposed for signal detection and synchronization [9]. Delayed correlation is suitable for fast but coarse timing synchronization. It comprises three branches, one for correlating parts A and C, another for correlating parts B and C, and the third for correlating

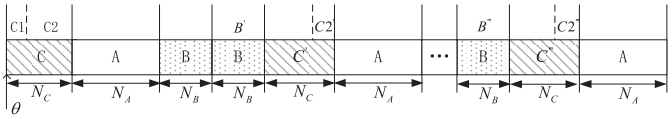

Fig. 1. Time-domain structure of the bootstrap.

parts A and B. After aggregating all three correlation values, the timing offset is estimated by locating the correlation peak, and meanwhile, the fine frequency offset (FFO) can be obtained by observing the phase shift of each correlation value.

Concerning signaling decoding, the cyclic shift indicating system parameters in TD can be detected by correlating the phase rotated reference sequence with received symbol in frequency domain. Assuming identical channel transfer functions (CTF) of adjacent bootstrap symbols, channel equalization can be applied to eliminate channel effects brought in by imperfect synchronization and multipath interference. However, the aforementioned assumption fails in fast time-selective fading channels and thereby the decoding performance will be deteriorated.

III. Proposed Structure

The proposed bootstrap inherits the TD structure of the standardized bootstrap, which adopts CAB-BCA repetition patterns as guard intervals. The originating sequence for the proposed bootstrap is a Zadoff-Chu (ZC) sequence modulated by a Gold sequence and the signaling can be conveyed simultaneously in both time and frequency domain, which possesses a lager capacity than the standardized bootstrap. For simplicity, TPS can be divided into three categories according to different applications, which are version signaling, common FD signaling and common TD signaling. In this subsection, the candidate FD sequence set, which constitutes the FD signal, is introduced first, and then the mapping from signaling to TD signal is detailed. The overall generation scheme of the adaptive bootstrap is sketched in Fig. 2.

The ZC sequence is generated as

$$Z(k) = e^{-j\pi 137 \frac{k(k+1)}{2039}}, \quad 0 \le k \le 2038 \tag{5}$$

where, sequence length, 2039, is the largest prime number smaller than 2048. In order to impose good periodic autocorrelation and cross-correlation properties on FD sequence, a Gold sequence set with a length of 2047, G, is generated by combining a pair of preferred Pseudo-Noise (PN) sequences. Each preferred PN sequence derives from a Linear Feedback Shift Register (LFSR) of length $l = 11$. The two shift registers are defined by the following two generator polynomials

$$g_1(x) = x^{11} + x^2 + 1 \tag{6}$$

$$g_2(x) = x^{11} + x^8 + x^5 + x^2 + 1 \tag{7}$$

After that, the generated Gold sequence set is BPSK modulated before combined with ZC sequence to generate the FD sequences. The family size of the generated Gold sequence set is 2048, and 1922 of it can be utilized to enable at most 64 bits signaling transmission as follows.

Similar to the generation of standardized bootstrap, a Grey code mapper without extra tolerance is utilized. For version signaling and common FD signaling, let $m_{N_b-1} \dots m_1 m_0$ be the binary representation of signaling bits in each symbol after Grey mapping. We have

$$m_i^n = \left(\sum_{k=0}^{N_b-1-i} b_k^n \right) \bmod 2 \tag{8}$$

wherein, N_b denotes the number of valid signaling bits in each signaling category. It is set to be 1 for version signaling ($n = 0$), 8 for common FD signaling ($0 < n < 8$) and 7 for common FD signaling ($n = 8$) in this paper. To build the connection between FD signaling and the Gold sequence set G_n, we define M_n^{abs} as the absolute index, which corresponds to 1922 available Gold sequences on a one-to-one basis.

$$M_n^{abs} = \begin{cases} M_n, & n = 0 \\ 2 + M_n + 256 \cdot (n-1), & n > 0 \end{cases} \tag{9}$$

where M_n is the decimal representation of signaling bits in (8). In this way, 1922 different Gold sequences can be distributed into as many as 9 symbols and 64 signaling bits can be carried by these symbols. The reason for employing different Gold sequences in adjacent several symbols is to eliminate side peaks in case of long multipath delays [12]. Actually, FD sequences can be reused, so the total signaling capacity is unlimited literally.

In terms of subcarrier mapping, considering the compatibility with the wireless communication system, the number of active subcarriers N (i.e., the truncating length) depends on the occupied bandwidth of current transmission system. Assuming a fixed subcarrier spacing of 3KHz, when the adaptive bootstrap is applied to a DTTB system with about 6MHz bandwidth, N is set as 2039. As a counterpart, N is set to be 1498 in a cellular system with 4.5MHz bandwidth. The FD signal mapped to subcarriers is presented as

$$S_n^{M_n^{abs}}(k) = \begin{cases} Z(k+1020) \cdot G_n^{M_n^{abs}}(1024+k), \\ \qquad -\lceil N/2 \rceil \le k \le -1 \\ Z(k+1019) \cdot G_n^{M_n^{abs}}(1023+k), \\ \qquad 1 \le k \le \lfloor N/2 \rfloor \\ 0, \qquad \text{otherwise} \end{cases} \tag{10}$$

When it comes to the common TD signaling, N_b is set to be 3 and the mapping scheme is exactly the same with [9]. After applying IFFT on $S_n^{M_n^{abs}}(k)$, the common TD signaling is conveyed by imposing cyclic shift on the TD signal $s_n^{M_n^{abs}}(t)$. The cyclically shifted time domain sequence $s_n^{(M_n^{abs}, T_n^{abs})}(t)$ can be obtained as

$$s_n^{(M_n^{abs}, T_n^{abs})}(t) = s_n^{M_n^{abs}}\left(\left(t + T_n^{abs} \right) \bmod 2048 \right) \tag{11}$$

where, T_n^{abs} is the absolute cyclic shift defined in [9]. An application of the proposed bootstrap design is sketched in Fig. 3.

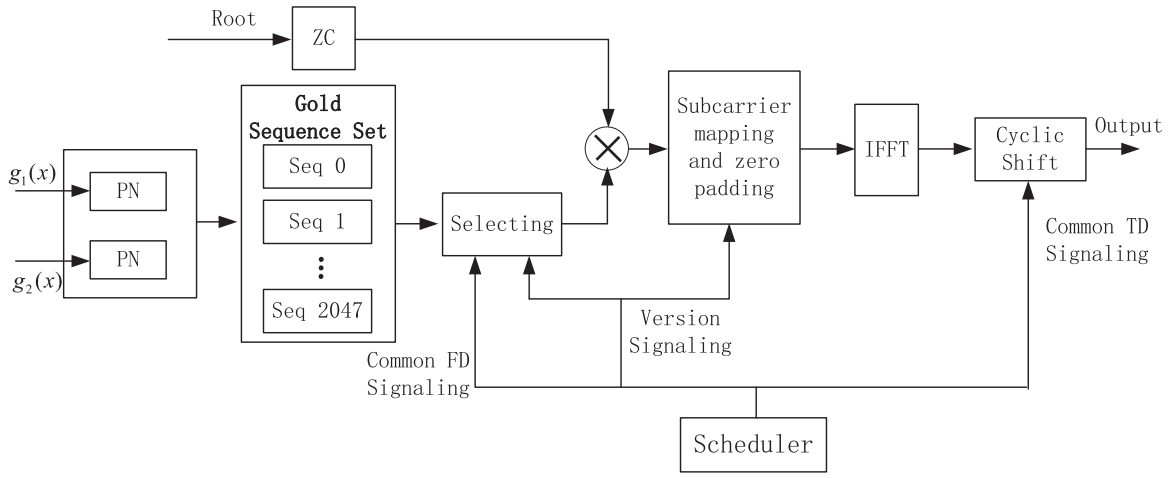

Fig. 2. Overall structure of the proposed bootstrap generator.

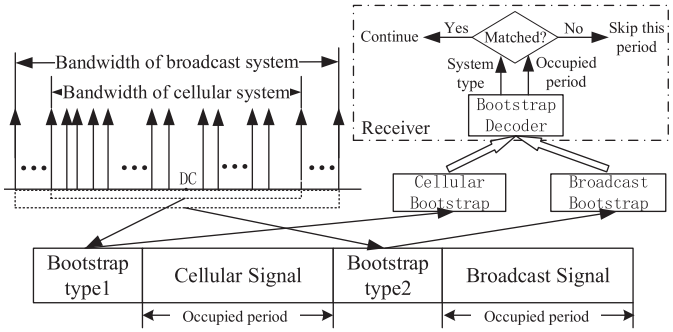

Fig. 3. Application of the proposed bootstrap design.

This bootstrap signal can precede diverse frames with different bandwidths, but they can be received in the same manner. Note that the second bootstrap symbol is recommended to carry the signaling about occupied time interval of subsequent load signal. In this way, mismatched receiver can be informed about the designated period to switch to another spectrum.

IV. Receiver Algorithms for Proposed Structure

A. Maximum Likelihood Function of Bootstrap With CAB-BCA Structure

ML synchronization aims at estimating both time and CFO, which maximize the probability of having received r_k. For easy explanation, the time-domain structure of the bootstrap is dissected as shown in Fig. 1. Some parts (e.g., part B) in the bootstrap have two correlative duplicates, which is different from the conventional preamble design (even P1) with at most one duplicate. As a consequence, we derive the log-likelihood function of this TD structure as the foundation for following synchronization improvement and groundwork for further research. By referring to [13] which approximated the time domain transmitted signal as Gaussian distributed, the conditional PDF of the first received block with θ time delay and ϕ CFO can be simplified as

$$f(r_k|\theta,\phi) \cong \prod_{k\in C1}\frac{f\left(r_k, r_{k+N_A}\right)}{f(r_k)f\left(r_{k+N_A}\right)}\prod_{k\in C2}\frac{f\left(r_k, r_{k+N_A}, r_{k+N_A+N_B}\right)}{f(r_k)f\left(r_{k+N_A}\right)f\left(r_{k+N_A+N_B}\right)} \quad (12)$$

For simplicity, let $\Phi = \frac{\phi}{N_A}$. The two-dimensional joint probability density function (PDF) in (12) can be written as

$$f\left(r_k, r_{k+N_A}\right) = \frac{1}{\pi^2\left(\delta_s^2+\delta_n^2\right)^2\left(1-\rho^2\right)}\exp\left\{\frac{-1}{\left(\delta_s^2+\delta_n^2\right)\left(1-\rho^2\right)} \cdot\left[|r_k|^2+\left|r_{k+N_A}\right|^2-2\rho\cdot\Re\left(r_k^* r_{k+N_A}e^{j2\pi\Phi N_A}\right)\right]\right\} \quad (13)$$

wherein, δ_n^2 and δ_s^2 represent the total power of AWGN and signal respectively, $\Re(\bullet)$ denotes the operation of taking real components.

Let us define $\zeta = (\delta_s^2+\delta_n^2)(1-3\rho^2+2\rho^3)$. The three-dimensional joint PDF of (12) can be written as (14) with $\rho = \frac{\delta_s^2}{\delta_s^2+\delta_n^2}$ and $n_c = \frac{k-\theta-16}{N_A}, k \in C2$.

$$\begin{aligned} f\left(r_k, r_{k+N_A}, r_{k+N_A+N_B}\right) &= \frac{1}{\left(\delta_s^2+\delta_n^2\right)^2\cdot\zeta} \cdot\exp\left\{-\frac{1}{\zeta}\left[\left(1-\rho^2\right)\left(|r_k|^2+\left|r_{k+N_A}\right|^2+\left|r_{k+N_A+N_B}\right|^2\right)\right.\right. \\ &+ 2\left(\rho^2-\rho\right)\left[\Re\left(r_k r^*_{k+N_A}e^{j2\pi\Phi N_a}\right)\right. \\ &+ \Re\left(r_k r^*_{k+N_A+N_B}e^{j2\pi[\Phi(N_A+N_B)+n_c]}\right) \\ &\left.\left.\left.+ \Re\left(r_{k+N_A} r^*_{k+N_A+N_B}e^{j2\pi(\Phi N_B+n_c)}\right)\right]\right]\right\} \end{aligned} \quad (14)$$

After neglecting the constant value contributing little to the maximization of (12) and taking the logarithmic operation,

we obtain the three-dimensional part of (12) as

$$\begin{aligned}
&\ln\left(\frac{f\left(r_k, r_{k+N_A}, r_{k+N_A+N_B}\right)}{f(r_k)f\left(r_{k+N_A}\right)f\left(r_{k+N_A+N_B}\right)}\right) \\
&= \frac{\left(|r_k|^2 + \left|r_{k+N_A}\right|^2 + \left|r_{k+N_A+N_B}\right|^2\right)}{\left(\delta_s^2 + \delta_n^2\right)} \\
&\quad - \frac{\left(1-\rho^2\right)\left(|r_k|^2 + \left|r_{k+N_A}\right|^2 + \left|r_{k+N_A+N_B}\right|^2\right)}{\left(\delta_s^2 + \delta_n^2\right)\left(\left(1-3\rho^2+2\rho^3\right)\right)} \\
&\quad - \frac{2\left(\rho^2-\rho\right)}{\left(\delta_s^2 + \delta_n^2\right)\left(1-3\rho^2+2\rho^3\right)} \\
&\quad \cdot\left\{\Re\left(r_k r^*_{k+N_A} e^{j2\pi(\Phi N_A)}\right) + \Re\left(r_k r^*_{k+N_A+N_B} e^{j2\pi[\Phi(N_A+N_B)+n_c]}\right)\right. \\
&\quad \left. + \Re\left(r_{k+N_A} r^*_{k+N_A+N_B} e^{j2\pi(\Phi N_B+n_c)}\right)\right\} \qquad (15)
\end{aligned}$$

After simplification, the log-likelihood function (LLF) can be regarded as a combination of two parts. For each k belonging to C1 in Fig. 1, the two-dimensional part of the LLF with mere C and A parts can be formulated as

$$\mathrm{A}(k) = \Re\left(r_k r^*_{k+N_A} e^{j2\pi(\Phi N_A)}\right) - \frac{\rho}{2}\left(|r_k|^2 + \left|r_{k+N_A}\right|^2\right) \quad (16)$$

For each k in C2, we have the three-dimensional part of the LLF in terms of C, A and B parts as

$$\begin{aligned}
\mathrm{B}(k) &= \Re\left(r_k r^*_{k+N_A+N_B} e^{j2\pi[\Phi(N_A+N_B)+n_c]}\right) \\
&\quad + \Re\left(r_k r^*_{k+N_A} e^{j2\pi(\Phi N_A)}\right) \\
&\quad + \Re\left(r_{k+N_A} r^*_{k+N_A+N_B} e^{j2\pi(\Phi N_B+n_c)}\right) \\
&\quad - \rho\left(|r_k|^2 + \left|r_{k+N_A}\right|^2 + \left|r_{k+N_A+N_B}\right|^2\right) \qquad (17)
\end{aligned}$$

By combining all samples with counterparts and neglecting all constant value, the overall LLF of four bootstrap symbols with C-A-B B-C-A structure can be formulated as

$$\begin{aligned}
\Lambda(\theta,\phi) &= |\gamma_1(\theta)|\cos(2\pi\phi + \angle\gamma_1(\theta)) \\
&\quad + |\gamma_2(\theta)|\cos\left(2\pi\phi\left(1+\frac{N_B}{N_A}\right) + \angle\gamma_2(\theta)\right) \\
&\quad + |\gamma_3(\theta)|\cos\left(2\pi\phi\frac{N_B}{N_A} + \angle\gamma_3(\theta)\right) - M_t(\theta) \qquad (18)
\end{aligned}$$

where

$$\gamma_1(\theta) = \left(\sum_{k\in C} r_k r^*_{k+N_A} + \sum_{k\in C'} r_k r^*_{k+N_A} + \sum_{k\in C''} r_k r^*_{k+N_A} + \sum_{k\in C'''} r_k r^*_{k+N_A}\right) \qquad (19)$$

$$\begin{aligned}
\gamma_2(\theta) &= \left(\sum_{k\in C2} r_k r^*_{k+N_A+N_B} e^{j2\pi n_c} + \sum_{k\in B'} r_k r^*_{k+N_A+N_B} e^{j2\pi n_c}\right. \\
&\quad \left. + \sum_{k\in B''} r_k r^*_{k+N_A+N_B} e^{j2\pi n_c} + \sum_{k\in B'''} r_k r^*_{k+N_A+N_B} e^{j2\pi n_c}\right) \qquad (20)
\end{aligned}$$

$$\begin{aligned}
\gamma_3(\theta) &= \left(\sum_{k\in C2} r_{k+N_A} r^*_{k+N_A+N_B} e^{j2\pi n_c} + \sum_{k\in B'} r_k r^*_{k+N_B} e^{j2\pi n_c}\right. \\
&\quad \left. + \sum_{k\in B''} r_k r^*_{k+N_B} e^{j2\pi n_c} + \sum_{k\in B'''} r_k r^*_{k+N_B} e^{j2\pi n_c}\right) \qquad (21)
\end{aligned}$$

$$\begin{aligned}
M_t(\theta) &= \frac{\rho}{2}\left[\sum_{k\in C1}\left(|r_k|^2 + \left|r_{k+N_A}\right|^2\right) + \sum_{k\in C2'}\left(|r_k|^2 + \left|r_{k+N_A}\right|^2\right)\right. \\
&\quad \left. + \sum_{k\in C2''}\left(|r_k|^2 + \left|r_{k+N_A}\right|^2\right) + \sum_{k\in C2'''}\left(|r_k|^2 + \left|r_{k+N_A}\right|^2\right)\right] \\
&\quad + \rho\left[\sum_{k\in C2}\left(|r_k|^2 + \left|r_{k+N_A}\right|^2 + \left|r_{k+N_A+N_B}\right|^2\right)\right. \\
&\quad + \sum_{k\in B'}\left(|r_k|^2 + \left|r_{k+N_B}\right|^2 + \left|r_{k+N_A+N_B}\right|^2\right) \\
&\quad + \sum_{k\in B''}\left(|r_k|^2 + \left|r_{k+N_B}\right|^2 + \left|r_{k+N_A+N_B}\right|^2\right) \\
&\quad \left. + \sum_{k\in B'''}\left(|r_k|^2 + \left|r_{k+N_B}\right|^2 + \left|r_{k+N_A+N_B}\right|^2\right)\right]. \qquad (22)
\end{aligned}$$

B. STO Estimator

This paper provides a non-coherent synchronizer based on (18) to achieve fast but coarse STO estimation. To avoid the harmful effects of power fluctuations of the received signal, normalization was commonly applied to the timing offset estimator [14], [15]. Assuming all CFO concerned terms and ρ to be 1, we maximize the normalized energy term $\Lambda(\theta)$ with respect to θ, obtaining

$$\hat{\theta} = \arg\max_{\theta}\{\Lambda(\theta)\} \qquad (23)$$

$$\Lambda(\theta) = \frac{|\gamma_1(\theta)| + |\gamma_2(\theta)| + |\gamma_3(\theta)|}{M_t(\theta)} - 1 \qquad (24)$$

where, $M_t(\theta)$ in (22) can be considered as an item incorporating the power of received signal.

C. Learning Based Spectrum Sensing

In [16], a sensing algorithm based on maximum energy (ME), which exploited the repetition structure of P1 symbol, was presented for DVB-T2 system. However, the threshold requires the prior knowledge of channel conditions including variance of noise, which is regularly unknown at the initial stage. To address this issue, the use of dynamic threshold based on the measured noise level in the received signal was investigated to enhance the probability of detection and decrease the probability of false alarm [17]. However, the power of noise can hardly be tracked in time-selective fading channels and the additional channel and noise estimator will introduce extra latency and computations [18]. In this paper, the maximum normalized energy (MNE) results from STO estimator are applied to spectrum sensing, which allows a fixed threshold distinguishing actual signal from interference in unknown channels. However, it is difficult to find an accurate theoretical threshold due to complex PDF of $\Lambda(\theta)$ and large amount of approximations like [19]. To this end, a linear classifier, SVM, is used to generate the fixed threshold T_{th} suitable for various channels without prior knowledge of channel parameters or noise estimator [20]. Valid signal with bootstrap and random signal are transmitted intermittently during the stipulated period. The MNE values $\Lambda(\hat{\theta})$ under different channel conditions act as training data X_{total}. A total framework of the generation process is shown in Fig. 4.

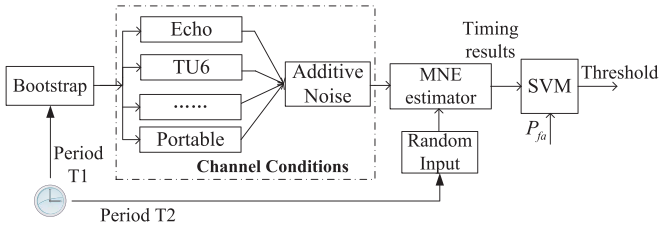

Fig. 4. Total framework of the SVM based threshold generator.

The target probability of false alarm P_{fa} is commonly predetermined and kept at the constant of P_{th} (0.01 for instance), because there is a tradeoff between probability of missed detection P_{md} and P_{fa}. In this paper, a scaling method preprocessing training data is used to adjust the model in reference to P_{th}, where scaling factor is generated iteratively by dichotomy.

Algorithm 1 shows the process for calculating the threshold T_{th} with SVM classification. N_r-fold cross-validation (CV) is conducted to evaluate the model. The initial scaling factor $\{S_{floor}, S_{mid}, S_{ceil}\}$ is set to be $\{\frac{8.5}{9}, \frac{8.5+9.5}{9.2}, \frac{9.5}{9}\}$. The number and index of test data in each validation are respectively represented as

$$N_{tlen} = \left\lfloor \frac{N_{totallen}}{N_{fold}} \right\rfloor, A_k = \{(k-1)\cdot N_{tlen}+1, \ldots, k\cdot N_{tlen}\} \tag{25}$$

Scaling operation is only applied to training data with label $-1(X_{total}^{(-1)})$, which corresponds to random signal rather than the bootstrap. After data processing, an available tool developed by Chih-Jen Lin, Libsvm, is used to generate the model by taking scaled training data ($X_{training}^{scaling}$), training data with label $+1(X_{training}^{(1)})$, and cost parameter (c) as input [21]. Cost parameter here belongs to $C = \{0.5, 2, 8, 32, 128, 512, 2048\}$. $P_{fa}^{(n,\alpha,c)}$ can be obtained by combining a predictor and validator of Libsvm, and meanwhile, a threshold in each iteration is generated as $T_{th}^{(n,\alpha,c)}$ with n denoting the index of iteration, α representing the scaling factor and c indicating the cost parameter. The candidate scaling factors are updated in a dichotomous way by comparing $P_{fa}^{(n,\alpha,c)}$ with P_{th}. In this way, $P_{fa}^{(n,\alpha,c)}$ will converges to the desired value P_{th} by adjusting the scaling factor α. At last, the resulting threshold is obtained as follows

$$\hat{T}_{th} = T_{th}^{(N_{iter},\hat{\alpha},\hat{c})} \tag{26}$$

$$\{\hat{\alpha},\hat{c}\} = \arg\min_{\{\alpha,c\}}\left\{|P_{fa}^{(N_{iter},\alpha,c)} - P_{th}|\right\} \tag{27}$$

where, N_{iter} is the number of iteration, which is set as 20 in this paper. The performance of detection and false alarm in different channel conditions are further presented in Section VI.

Algorithm 1: Threshold Acquisition by Scaled-SVM

Input: N_{iter}, $X_{total}^{(-1)}$, $X_{total}^{(1)}$, $\{S_{floor}, S_{mid}, S_{ceil}\}$, C
Output: Threshold $\hat{T}_{th}$

for *all* $n \in \{1, 2, \ldots N_{iter}\}$ **do**
  for *all* $\alpha \in \{S_{floor}, S_{mid}, S_{ceil}\}$ **do**
    $X_{total}^{scaling} \leftarrow X_{total}^{(-1)} \cdot \alpha$;
    for *all* $c \in C$ **do**
      for *all* $k \in \{1, 2, \ldots N_{fold}\}$ **do**
        $X_{test}^{scaling} \leftarrow \{X_{total}^{scaling}(A_k)\}$;
        $X_{test}^{(1)} \leftarrow \{X_{total}^{(1)}(A_k)\}$;
        $X_{trainig}^{scaling} \leftarrow \{X_{total}^{scaling}\} - \{X_{test}^{scaling}\}$;
        $X_{trainig}^{(1)} \leftarrow \{X_{total}^{(1)}\} - \{X_{test}^{(1)}\}$;
        $model = \textbf{svmtrain}(X_{trainig}^{scaling}, X_{trainig}^{(1)}, c)$;
        $X_{test}^{(-1)} \leftarrow \{X_{total}^{(-1)}(A_k)\}$;
        $Dec_k^{(-1)} = \textbf{svmpredict}(X_{test}^{(-1)}, model)$;
      end
      $P_{fa}^{(n,\alpha,c)} = \textbf{Val}(Dec_1^{(-1)}, \ldots Dec_{N_{fold}}^{(-1)})$;
      $T_{th}^{(n,\alpha,c)} = \textbf{Bound}(model)$;
    end
    $P_{fa}^{(n,\alpha)} \leftarrow \arg\min_{c\in C}\{|P_{fa}^{(n,\alpha,c)} - P_{th}|\}$;
  end
  if $P_{fa}^{(n,S_{mid})} < P_{th} \le P_{fa}^{(n,S_{floor})}$ **then**
    $S_{ceil} \leftarrow S_{mid}$, $S_{mid} \leftarrow (S_{floor} + S_{ceil})/2$;
  else
    $S_{floor} \leftarrow S_{mid}$, $S_{mid} \leftarrow (S_{floor} + S_{ceil})/2$;
  end
end
$\{\hat{\alpha},\hat{c}\} = \arg\min_{\{\alpha,c\}}\{|P_{fa}^{(N_{iter},\alpha,c)} - P_{th}|\}$;
$\hat{T}_{th} \leftarrow T_{th}^{(N_{iter},\hat{\alpha},\hat{c})}$;

D. FFO Refinement-Aggregated vs Differential

In order to find the maximum of (18), we have following assumptions

$$\begin{aligned}\cos(2\pi\phi + \angle\gamma_1) &= \cos\left(2\pi\phi\left(1+\frac{N_B}{N_A}\right) + \angle\gamma_2\right)\\ &= \cos\left(2\pi\phi\frac{N_B}{N_A} + \angle\gamma_3\right) = 1\end{aligned} \tag{28}$$

so we have

$$2\pi\phi + \angle\gamma_1 = 2\pi k_1 \tag{29}$$

$$2\pi\phi\left(1+\frac{N_B}{N_A}\right) + \angle\gamma_2 = 2\pi k_2 \tag{30}$$

$$2\pi\phi\frac{N_B}{N_A} + \angle\gamma_3 = 2\pi k_3 \tag{31}$$

where k_1, k_2, k_3 are integer numbers. (29), (30) and (31) can be combined in a variety of ways, which corresponds to different CFO estimation schemes. By aggregating all equations above, the estimated FFO candidate can be derived as

$$\phi\left(\hat{k}\right) = \frac{2\pi\hat{k} - (\angle\gamma_1 + \angle\gamma_2 + \angle\gamma_3)}{(1+N_B/N_A)\cdot 4\pi} \tag{32}$$

Considering that ϕ is within $(-0.5, 0.5]$, so $\hat{k}$ belongs to $\{-3, -2, -1, 0, 1, 2, 3\}$. The FFO can be estimated by substituting k into (32) where k is derived as follows

$$k = \arg\max_{\hat{k}}\left\{\Lambda\left(\phi\left(\hat{k}\right)\right)\right\} \tag{33}$$

When the estimated FFO candidate $\phi(\hat{k})$ is differentially derived as follows, the FFO estimator is equivalent to that in [9].

$$\phi\left(\hat{k}\right) = \frac{2\pi\hat{k} - (\angle\gamma_1 + \angle\gamma_2 - \angle\gamma_3)}{4\pi} \tag{34}$$

By comparing denominators of (32) and (34), a better performance of about $(10 \cdot \log_{10}^{(1+N_B/N_A)^2})$dB can be achieved by exploiting the proposed aggregated method from (32).

The CFO estimation performance can be evaluated by referring to the Cramer-Rao Lower Bound (CRLB), which represents the error variance of the estimated CFO. Combining all samples and following the derivations of [22], we obtain (35) in the case of ideal timing synchronization.

$$\begin{aligned}
&E\left\{\frac{\partial^2\Lambda(\phi)}{\partial\phi^2}\right\} \\
&= 4\pi^2 \cdot \frac{2\left(\rho^2-\rho\right)}{\left(\delta_s^2+\delta_n^2\right)\left(1-3\rho^2+2\rho^3\right)} \\
&\quad \cdot\left\{N_B \cdot \left[1+\left(1+\frac{N_B}{N_A}\right)^2+\left(\frac{N_B}{N_A}\right)^2\right]\right\} \\
&\quad - \frac{2\rho}{\left(\delta_s^2+\delta_n^2\right)\left(1-\rho^2\right)} \cdot (N_C - N_B) \\
&= -4\pi \cdot \left\{N_B \cdot \left[1+\left(1+\frac{N_B}{N_A}\right)^2+\left(\frac{N_B}{N_A}\right)^2\right] \cdot \frac{2 \cdot SNR^2}{1+3 \cdot SNR}\right. \\
&\qquad \left. + (N_C - N_B) \cdot \frac{2 \cdot SNR^2}{1+2 \cdot SNR}\right\}
\end{aligned} \tag{35}$$

where, $\Lambda(\phi)$ is the LLF of each bootstrap symbol from (12). As a result, we have the CRLB for an OFDM symbol with CAB or BCA structure as $\frac{-1}{E\{\frac{\partial^2\Lambda(\phi)}{\partial\phi^2}\}}$.

E. IFO Estimation and Version Signaling Decoding

The decoding of version signaling is performed in conjunction with IFO estimation. To exploit all possible signal, the received first bootstrap symbol $r(t)$ with 1024 extra samples in addition to pre-/post-fix is converted to the FD by the 4096-point FFT after FFO compensation, yielding $R_0(k)$.

Firstly, let the circularly shifted FFT result correlate with candidate local sequences $S_M(k)$, which has a length of 4096 by zero padding. To eliminate the distortion brought in by residual timing offset, IFFT operation as [23] is adopted. So we have

$$\begin{aligned}
\Gamma_{\Delta k}^{M}(n) = \frac{1}{4096}\sum_{k=0}^{4095} R_0(k+2\cdot\Delta k)\cdot S_M^*(k)e^{j\frac{2\pi nk}{4096}}, \\
0 \le n < 4096
\end{aligned} \tag{36}$$

where, $\Delta k \in [-N : N]$, N is the range of the IFO estimator. M indicating the version signaling belongs to $\{0, 1\}$. Note that the cyclic shift in (36) is two times of Δk because of the double FFT size. And then, find the peak value $\Upsilon_M(\Delta k)$ of (36) corresponding to each candidate version signaling M and candidate IFO Δk as follows:

$$\Upsilon_M(\Delta k) = \max_n\left\{\left|\Gamma_{\Delta k}^{M}(n)\right|\right\} \tag{37}$$

The version signaling can be estimated by finding the maximum of (37) with respect to M as follows

$$\hat{M} = \arg\max_M\{\max[\Upsilon_M(\Delta k)]\} \tag{38}$$

And then, the estimated IFO can be obtained as

$$\Delta\hat{k} = \arg\max_{\Delta k}\left\{\Upsilon_{\hat{M}}(\Delta k)\right\} \tag{39}$$

It is worth noting that the bandwidth of received signal is unknown for IFO estimator and version signaling decoder at this stage. Even though, mismatched receivers are still able to achieve IFO estimation and signaling decoding because the proposed bootstrap signal is derived in a compatible way as described in Section III.

F. Two-Dimensional Signaling Decoder

After symbol timing synchronization and CFO correction, the OFDM symbol converted to frequency domain by 2048-point FFT operation after prefix and postfix removal is represented as $R_i(k)$, where i denotes the index of the bootstrap symbol. For signaling decoding, a variant of iterative scheme, which can minimize the effects of channel distortion, is utilized. The IFFT operation similar to ICFO estimator above is used other than the correlation-based scheme in [9]. In this way, FD signaling can be decoded regardless of TD signaling at the first stage. After that, TD signaling decoding can be achieved in exactly the same way with [9]. A flowchart of the proposed scheme is shown in Fig. 5 and a detailed explanation is presented as follows.

At first, multiply the ith received FD symbol $R_i(k)$ by the conjugation of the 256 candidate local reference sequences $S_i^M(k)$ in (10). After passing through a multipath control filter, an IFFT operation is applied to the multiplication of current candidate CTF $H_i(k, m)$ and actual CTF of previous symbol $H_{i-1}^*(k, \hat{M}_{i-1}, \hat{T}_{i-1}^{abs})$. Similar to the version signaling decoder, we have the normalized result as follows

$$\Gamma^M(l) = \frac{1}{\eta}\sum_{k=0}^{2047} H_i(k, M)\cdot H_{i-1}^*\left(k, \hat{M}_{i-1}, \hat{T}_{i-1}^{abs}\right)\cdot e^{j\frac{2\pi lk}{2048}} \tag{40}$$

where l belongs to $[0, 2048)$, η is the number of active subcarriers, which is 2039 for 6MHz system and 1498 for 4.5MHz system. And then, find the peak value $\Psi(M)$ of (40) corresponding to each candidate FD signaling M as follows:

$$\Psi(M) = \max_l\left\{\left|\Gamma^M(l)\right|\right\} \tag{41}$$

whereupon, the estimated common FD signaling can be represented as

$$\hat{M}_i = \arg\max_M\{\Psi(M)\} \tag{42}$$

After finding the designated sequence for current symbol, common TD signaling decoder is exactly the same with [9]. The absolute cyclic shift $\hat{T}_i^{abs}$ can be obtained as

$$\hat{T}_i^{abs} = \arg\max_{T\in[0:2047]}\left\{\left|\sum_{k=0}^{2047} R_i(k)\left[S_i^{\hat{M}_i}(k)\exp\left(-\frac{j2\pi kT}{2048}\right)\right]^*\right|\right\} \tag{43}$$

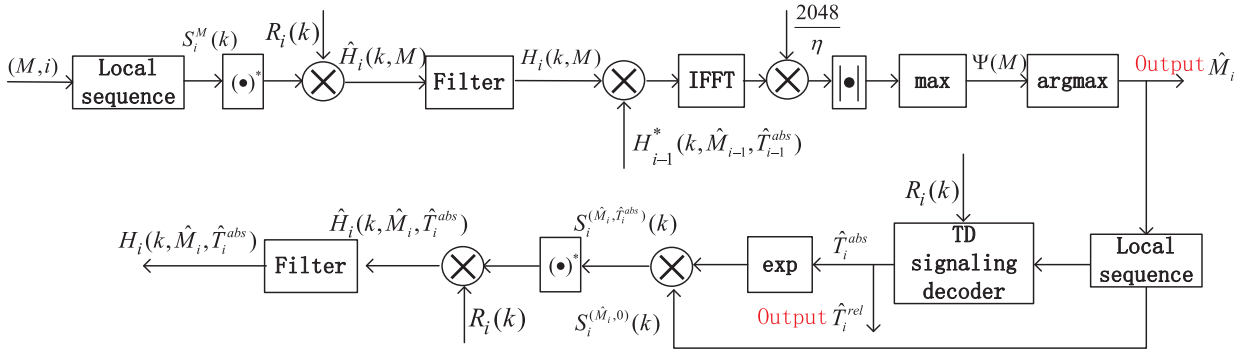

Fig. 5. FD and TD signaling decoder.

After that, the filtered actual CTF of current symbol, which can be used for signaling decoding of next symbol, is obtained as

$$H_i\left(k,\hat{M}_i,\hat{T}_i^{abs}\right)=Fil\left[R_i(k)\cdot\left(S_i^{\left(\hat{M}_i,\hat{T}_i^{abs}\right)}(k)\right)^*\right] \tag{44}$$

where, $Fil[\bullet]$ represents the multipath control filter proposed in [12].

The FD signaling decoder is insensitive to TD cyclic shift brought in by either TD signaling or residual STO, because the IFFT operation adopted essentially explores all TD cyclic shifts and locate the correct peak position in TD as analyzed in [23]. As a result, TPS can be conveyed in both FD and TD, which allows larger signaling capacity. In this paper, the decoding performance with a capacity of 11 bits each symbol, 8 bits FD signaling and 3 bits TD signaling, is investigated by simulation.

V. Performance Analysis

This section firstly performs theoretical analysis on both FD and TD signaling decoder over AWGN channel. Then the signaling decoding performances of the standardized and proposed bootstrap in severe channels, specifically channels with strong multipath and fast time-variation, are evaluated and compared.

A. Tractable Signaling Error Rate (SER) of the Proposed Bootstrap

Let m denote the actual index of the modulating sequence and Δl be the TD absolute cyclic shift. Assuming perfect timing synchronization and CFO correction, under AWGN channel, (40) can be simplified like [12], obtaining

$$\begin{aligned}\Gamma_n(l)&=\frac{1}{\eta}\left\{\sum_{k=0}^{2047}\left[S_m(k)e^{-j\frac{2\pi k\Delta l}{2048}}+N(k)\right]\cdot S_n^*(k)e^{j\frac{2\pi kl}{2048}}\right\}\\&=\frac{1}{\eta}\left\{\sum_{k=0}^{2047}\left[S_m(k)\cdot S_n^*(k)e^{j\frac{2\pi k(l-\Delta l)}{2048}}\right]\right.\\&\qquad\left.+\left[N(k)\cdot S_n^*(k)e^{j\frac{2\pi kl}{2048}}\right]\right\}\end{aligned} \tag{45}$$

where, $S_m(k)$ is the designated FD sequence, $S_n(k)$ is the candidate sequences with n belonging to $\{0,1,\ldots,255\}$, l is the candidate TD cyclic shifts. When $m=n$, we have

$$\Gamma_{m=n}=\begin{cases}\sum_{k=0}^{2047}\left[|S_n(k)|^2+N(k)\cdot S_n^*(k)e^{j\frac{2\pi k\Delta l}{2048}}\right]/\eta, l=\Delta l\\ \sum_{k=0}^{2047}\left[N(k)\cdot S_n^*(k)e^{j\frac{2\pi kl}{2048}}\right]/\eta, l\neq\Delta l\end{cases} \tag{46}$$

with $\sum_{k=0}^{2047}e^{j\frac{2\pi kL}{2048}}=0,(L\neq 0)$. Similarly, (45) can be described as (47) in case of $m\neq n$.

$$\Gamma_{m\neq n}=\begin{cases}\frac{1}{\eta}\sum_{k=0}^{2047}\left\{\left[S_m(k)\cdot S_n^*(k)\right]\right.\\ \qquad\left.+\left[N(k)\cdot S_n^*(k)e^{j\frac{2\pi k\Delta l}{2048}}\right]\right\}, l=\Delta l\\ \frac{1}{\eta}\sum_{k=0}^{2047}\left\{\left[S_m(k)\cdot S_n^*(k)e^{j\frac{2\pi k(l-\Delta l)}{2048}}\right]\right.\\ \qquad\left.+\left[N(k)\cdot S_n^*(k)e^{j\frac{2\pi kl}{2048}}\right]\right\}, l\neq\Delta l\end{cases} \tag{47}$$

The real part and imaginary part of $N(k)$ are random variables (RVs) which are subjected to zero-mean Gaussian distribution and independent of each other. It is clear that the real part and imaginary part of $\Gamma_n(l)$ are also subjected to Gaussian distributions and independent of each other.

Let us define the following variables in (47)

$$\beta_{\mathrm{Re}}=\Re\left\{\sum_{k=0}^{2047}S_m(k)\cdot S_n^*(k)\right\} \tag{48}$$

$$\beta_{Im}=\Im\left\{\sum_{k=0}^{2047}S_m(k)\cdot S_n^*(k)\right\} \tag{49}$$

$$\alpha_{\mathrm{Re}}=\Re\left\{\sum_{k=0}^{2047}S_m(k)\cdot S_n^*(k)e^{j\frac{2\pi k(l-\Delta l)}{2048}}\right\} \tag{50}$$

$$\alpha_{\mathrm{Im}}=\Im\left\{\sum_{k=0}^{2047}S_m(k)\cdot S_n^*(k)e^{j\frac{2\pi k(l-\Delta l)}{2048}}\right\} \tag{51}$$

Considering good cross-correlation property of frequency-domain sequences, we can assume that $\beta_{\mathrm{Re}}\approx\beta_{Im}\approx\alpha_{\mathrm{Re}}\approx\alpha_{\mathrm{Im}}\approx 0$. So the RV $\Gamma_n(l)$ has following features

$$\Re\left\{\Gamma_{m=n}^{l=\Delta l}\right\}\sim N\left(1,\frac{\delta_n^2}{2\cdot\eta}\right),\ \Im\left\{\Gamma_{m=n}^{l=\Delta l}\right\}\sim N\left(0,\frac{\delta_n^2}{2\cdot\eta}\right) \tag{52}$$

$$\Re\left\{\Gamma_{m=n}^{l\neq\Delta l}\right\}\sim N\left(0,\frac{\delta_n^2}{2\cdot\eta}\right),\ \Im\left\{\Gamma_{m=n}^{l\neq\Delta l}\right\}\sim N\left(0,\frac{\delta_n^2}{2\cdot\eta}\right) \tag{53}$$

$$\Re\left\{\Gamma_{m\neq n}^{l=\Delta l}\right\} \sim N\left(0, \frac{\delta_n^2}{2\cdot\eta}\right),\ \Im\left\{\Gamma_{m\neq n}^{l=\Delta l}\right\} \sim N\left(0, \frac{\delta_n^2}{2\cdot\eta}\right) \quad (54)$$

$$\Re\left\{\Gamma_{m\neq n}^{l\neq\Delta l}\right\} \sim N\left(0, \frac{\delta_n^2}{2\cdot\eta}\right),\ \Im\left\{\Gamma_{m\neq n}^{l\neq\Delta l}\right\} \sim N\left(0, \frac{\delta_n^2}{2\cdot\eta}\right) \quad (55)$$

In (52), (53), (54), and (55), $|\Gamma_{m=n}^{l=\Delta l}|$, $|\Gamma_{m=n}^{l\neq\Delta l}|$, $|\Gamma_{m\neq n}^{l=\Delta l}|$ and $|\Gamma_{m\neq n}^{l\neq\Delta l}|$ are subjected to chi-square distribution and the probability density function (PDF) are denoted as

$$f_{\Gamma_{m=n}^{l=\Delta l}}(y) = \frac{1}{2\delta^2} e^{-\frac{y+1}{2\delta^2}} I_0\left(\frac{\sqrt{y}}{\delta^2}\right) \quad (56)$$

$$f_{\Gamma_{m=n}^{l\neq\Delta l}}(y) = f_{\Gamma_{m\neq n}^{l=\Delta l}}(y) = f_{\Gamma_{m\neq n}^{l\neq\Delta l}}(y) = \frac{1}{2\delta^2} e^{-\frac{y}{2\delta^2}} \quad (57)$$

where $\delta^2 = \frac{\delta_n^2}{2\eta}$ and $I_0(\bullet)$ is the zero-order modified Bessel function of the first kind. For notational brevity, $f_{\Gamma_{m\neq n}^{l\neq\Delta l}}(y)$ and $f_{\Gamma_{m\neq n}^{l=\Delta l}}(y)$ can be combined as $f_{\Gamma_{m\neq n}}(y)$.

Firstly, we derive the FD SER representation regardless of the TD signaling as follows. Given RV $Z_1{}^{FD}(n) = \max_{0\le l\le 2047} |\Gamma_{m\neq n}(l)|$, its PDF is

$$f_{Z_1{}^{FD}(n)}(z_1) = \frac{2048}{2\delta^2}\left(1 - e^{-\frac{z_1}{2\delta^2}}\right)^{2047} e^{-\frac{z_1}{2\delta^2}},\ z_1 > 0 \quad (58)$$

where the superscript *FD* indicates that the TD signaling l has been removed by the maximization operation. Similarly, let $Z_{peak}^{FD} = \max_{0\le l\le 2047} |\Gamma_{m=n}(l)|$, its PDF is

$$f_{Z_{peak}^{FD}}(z) = \frac{\partial P_{peak}(z)}{\partial z},\ z > 0 \quad (59)$$

$$P_{peak}(z) = \left(\int_0^z \frac{1}{2\delta^2} e^{-\frac{y}{2\delta^2}} dy\right)^{2047} \cdot \left(\int_0^z \frac{1}{2\delta^2} e^{-\frac{y+1}{2\delta^2}} I_0\left(\frac{\sqrt{y}}{\delta^2}\right) dy\right),\ z > 0 \quad (60)$$

Furthermore, let $Z_{\text{out}}^{FD} = \max_{0\le n\le 255, m\neq n} |Z_1{}^{FD}(n)|$, its PDF can be formulated as

$$f_{Z_{out}^{FD}}(y) = \frac{2048\cdot 255}{2\delta^2}\left(1 - e^{-\frac{y}{2\delta^2}}\right)^{2048\cdot 255-1} e^{-\frac{y}{2\delta^2}},\ y > 0 \quad (61)$$

From (59) and (61), the FD SER can be written as

$$P\left(Z_{peak}^{FD} < Z_{out}^{FD}\right) = 1 - \int_0^{+\infty}\left(\int_0^z f_{Z_{out}^{FD}}(y)dy\right) f_{Z_{peak}^{FD}}(z)dz \quad (62)$$

Afterwards, we provide the TD SER representation by making some minor modifications to the above derivation. For notational brevity, let B and $\overline{B}$ (i.e., (62)) represent the events with correct and false FD signaling decoding respectively. Similarly, A and $\overline{A}$ correspond to correct and false TD signaling decoding. According to the law of total probability, the TD SER can be written as

$$P^{TD}(\overline{A}) = P(\overline{A}|B)P(B) + P(\overline{A}|\overline{B})P(\overline{B}) \quad (63)$$

Notice that, to provide larger tolerance against any distortion, we only utilize 8 out of 2048 TD cyclic shifts to enable 3-bit TD signaling transmission in this paper. Therefore, $\overline{A}$ occurs when $\lceil l/256\rceil \neq \lceil \Delta l/256\rceil$. Refer to (59), (61), (62), we can easily obtain

$$P(\overline{A}|B) = 1 - \int_0^{+\infty}\left(\int_0^z f_{Z_{out}^{TD}}(y)dy\right) f_{Z_{peak}^{TD}}(z)dz \quad (64)$$

where

$$f_{Z_{out}^{TD}}(y) = \frac{256\cdot 7}{2\delta^2}\left(1 - e^{-\frac{y}{2\delta^2}}\right)^{256\cdot 7-1} e^{-\frac{y}{2\delta^2}},\ y > 0 \quad (65)$$

$$f_{Z_{peak}^{TD}}(z) = \frac{\partial P_{peak}(z)}{\partial z},\ z > 0 \quad (66)$$

$$P_{peak}(z) = \left(\int_0^z \frac{1}{2\delta^2} e^{-\frac{y}{2\delta^2}} dy\right)^{255} \cdot \left(\int_0^z \frac{1}{2\delta^2} e^{-\frac{y+1}{2\delta^2}} I_0\left(\frac{\sqrt{y}}{\delta^2}\right) dy\right),\ z > 0 \quad (67)$$

And

$$P(\overline{A}|\overline{B}) = 1 - \int_0^{+\infty}\left(\int_0^z f_{Z_{out}^{TD}}(y)dy\right) f_{Z_{\overline{peak}}^{TD}}(z)dz \quad (68)$$

where

$$f_{Z_{\overline{peak}}^{TD}}(z) = \frac{256}{2\delta^2}\left(1 - e^{-\frac{z}{2\delta^2}}\right)^{255} e^{-\frac{z}{2\delta^2}},\ y > 0 \quad (69)$$

The theoretical FD and TD SER in (62) and (63) are depicted in Fig. 6 and corresponding simulation results are also presented for comparison. All the integral operations above are accomplished by using the numerical integration of MATLAB. From the Bayesian perspective, (63) can be rewritten as

$$P^{TD}(\overline{A}) = P(B|\overline{A})P(\overline{A}) + P(\overline{A}|\overline{B})P(\overline{B}) \quad (70)$$

Intuitively, $P(\overline{A}|\overline{B})$ approximates 1 and $P(B|\overline{A})$ is close to 0 in flat channel due to the absence of correlation peak given $\overline{B}$ and $\overline{A}$. As a result, $P^{TD}(\overline{A}) \approx P(\overline{B})$, which is in line with the results in Fig. 6. However, this assumption and inference will fail in the presence of strong multipath signals, which will be discussed in the following and Section V.

B. Performance Evaluation of the Standardized and Proposed Bootstrap in Severe Channels

Bootstrap symbol aims to act as a common entry point for various wireless systems, therefore, some severe channels in both broadcast and cellular scenarios need to be dealt with. However, it is quite difficult to derive a closed-form representation of the signaling performance in severe channels on account of many unknown random variables. Consequently, we apply qualitative analysis about the impact of strong multipath and fast time-variation separately by investigating the signaling performance in two typical channels, 0db echo channel for strong multipath and TU6 channel for fast time-variation.

Signaling transmission through time-domain cyclic shift, which is adopted by the standardized bootstrap, suffers from considerable performance degradation in echo channel because of significant side lobes brought in by strong

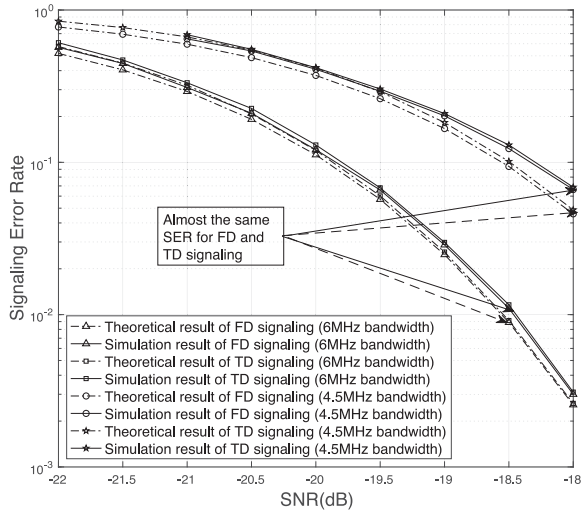

Fig. 6. SER simulation results of the adaptive bootstrap with different bandwidths in comparison with the theoretical bound over AWGN channel.

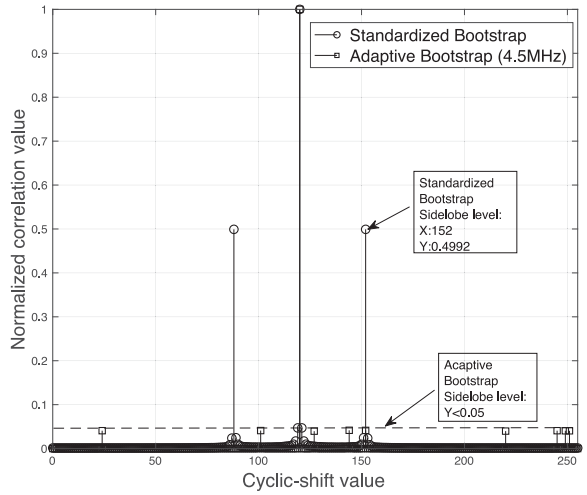

Fig. 7. Decoding metric comparison under 0dB echo channel.

multipath [12]. Specifically, two significant side lobes can be detected at $l = \langle \Delta l \pm (\tau/8) \rangle_{256}$ in the presence of a strong multipath component with delay τ. Comparatively, the multipath component contributes little to the sidelobes of the mutual correlation result in (40) as indicated by (47). Fig. 7 compares the proposed bootstrap with the standardized one in terms of correlation results on condition that the second path has a delay of 256 samples. Significant sidelobes can be observed at $\{120 \pm 32\}$ for the standardized bootstrap, whereas the proposed bootstrap has considerably smaller sidelobes. Observed from Fig. 7, the assumption about $P(B|\overline{A})$ in Section V-A collapse, because there are still some correlation peaks at false locations.

To reveal the time-selective fading impairment on signaling decoding of the standardized and proposed bootstrap, a typical channel in mobile scenario,TU6 with high-Doppler shift f_d, is investigated by nonlinear fitting. There is an assumption for standardized bootstrap that CTFs of adjacent symbols are the

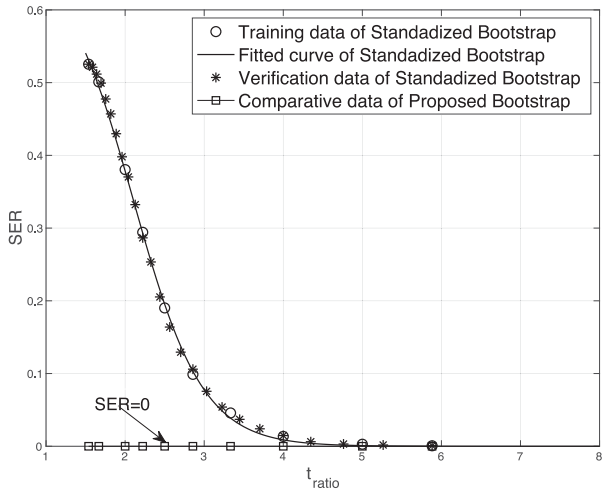

Fig. 8. Fitting performance with respect to time ratios and SER.

same [9]. However, this assumption cannot be put to work when symbol duration is comparable to coherence time.

The time duration of two bootstrap symbols t_{sym} and the coherence time t_{corr}, which is inversely proportional to the Doppler spreading, can be represented respectively as

$$t_{sym} = \frac{2 \cdot N_{sym}}{f_s}, t_{corr} \propto \frac{1}{f_d} \tag{71}$$

where, $N_{sym} = 3072$ and $f_s = 6.144 \cdot 10^6$. Then we get the time ratio as

$$t_{ratio} = \frac{t_{corr}}{t_{sym}} = \frac{f_s}{f_d \cdot 2 \cdot N_{sym}} \tag{72}$$

Through observation, the SER with parameter t_{ratio} can be fitted by

$$\overrightarrow{SER^{a}}(t_{ratio}) = \frac{a(4)}{a(1) + a(2) \cdot e^{a(3) \cdot t_{ratio}}} \tag{73}$$

Firstly, we resort to Monte Carlo to generate a training set with several time ratios as $\{t_{ratio}^{\text{training}}, SER^{\text{training}}\}$. Then the estimated parameter vector can be derived from nonlinear curve-fitting with least squares criterion, which is

$$\hat{a} = \arg\min_{\vec{a}} \sum \left[\overrightarrow{SER^{a}}\left(t_{ratio}^{\text{training}}\right) - SER^{\text{training}} \right]^2 \tag{74}$$

Specifically, we first generate a training set with 10 pairs in TU6 channel, whereupon the estimated parameter vector in (74) can be derived by lsqcurvefit function of MATLAB and obtained as $[1.9581, 0.0161, 2.2813, 1.3254]$. And then, a verification set $\{t_{ratio}^{\text{verification}}, SER^{\text{verification}}\}$ with 25 pairs is generated for model verification and the performance is shown in Fig. 8. Simulation results reveal that signaling transmission in TD requires strong coherence of two adjacent symbols. The probability of false decoding almost increases exponentially along with the decrease of t_{ratio}. Fig. 9 compares the decoding metrics between the standardized bootstrap and the proposed bootstrap when CTFs of adjacent symbols are independent of each other. Even in absence of noise, a great deal of significant side peaks can be observed for the standardized bootstrap. Comparatively, no significant side peaks can be observed for

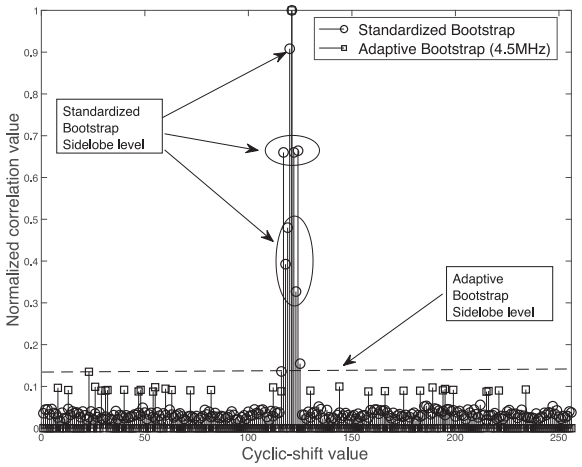

Fig. 9. Decoding metric comparison under fast time-selective fading channel.

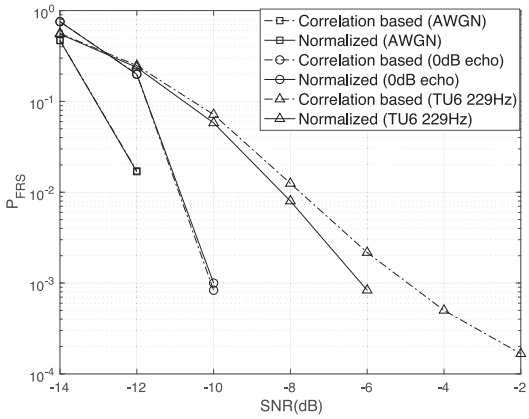

Fig. 10. Probability of failed synchronization for the bootstrap.

the proposed bootstrap, which means independent CTF has little impact on the proposed decoding metric. Moreover, Fig. 8 demonstrates that short coherence time will not lead to false decoding of the proposed bootstrap.

VI. Simulation Result

In this section, the performance improvement of the proposed bootstrap is evaluated in terms of error rate of synchronization, spectrum sensing and signaling decoding. The number of trials is set to enable that the number of failures (including each failed synchronization, detection and decoding) is 100. Four typical channels are considered. A COST207 TU6 channel with a maximum Doppler frequency of 229 Hz is adopted to verify the improvement on symbol timing synchronization in case of time-selective fading channel. For spectrum sensing, the performance is assessed in terms of the probability of missed detection P_{md}. To evaluate the combined impact of strong multipath and fast time-variation on the decoding performances (including version signaling), Mobile SFN channel consisting of two-path TU6 channels are introduced.

A. Synchronization and Spectrum Sensing

In this paper, we evaluate the symbol timing synchronization by the failure rate of synchronization P_{FRS} as described in [24].

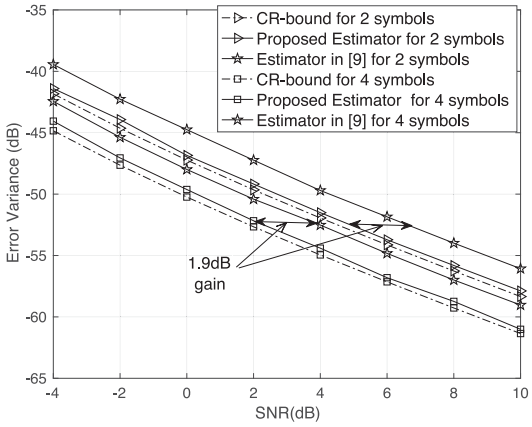

Fig. 11. Variance of CFO estimation error and CRLB.

The frame is assumed to be correctly synchronized if the error in time is lower than N_c samples, so P_{FRS} can be expressed as

$$P_{FRS} = P\left\{|\hat{\theta} - \theta| > N_c\right\} \tag{75}$$

where $\hat{\theta}$ and θ denote the estimated and actual STO respectively. N_c is the length of the cyclic prefix, which is 520 for the bootstrap. Fig. 10 compares the synchronization performance between the CBS in [9] and the MNE scheme as a function of the SNR. We observe that the two schemes have similar performances in static channels like AWGN and 0dB echo channel, whereas the normalized method outperforms the CBS in TU6 channel with a high Doppler shift.

For FFO estimation, a comparison between the estimator in [9] and the proposed estimator are displayed in Fig. 11. To investigate the performance improvement with respect to the bootstrap duration, experiments are conducted by using the bootstrap with two and four OFDM symbols in AWGN channel. We also report the CRLB for these two cases. We observe that the proposed estimator has a much closer curve to the CRLB and about 1.9 dB gain can be achieved as predicted in Section IV. Moreover, about 3dB gain can be observed by the four-symbol estimator, because it utilizes twice as many samples as the two-symbol one.

Fig. 12 and Fig. 13 compare the signal detection performance among the static correlation-based scheme with fixed threshold, the dynamic correlation-based scheme with variable threshold and the proposed scheme combining normalization and SVM. The fixed threshold is derived with the lowest operating SNR of -11dB [16] and the dynamic threshold is generated assuming perfect noise estimation, which is regarded as the benchmark. The probability of false alarm is a fixed 0.01. For the proposed scheme, the training data serving as the input of the SVM are generated in the case of 3 channel types (AWGN, 0dB echo and TU6) and 3 SNR values (-14dB, -8dB and -2dB). From Fig. 12, it is noticed that the benchmark and the proposed scheme have a consistent threshold and stable P_{fa} in various cases. However, P_{fa} of the static correlation-based scheme decreases with an increase in SNR, because the threshold is obtained in environments with low SNR. However, this threshold is too high for scenario with higher SNR to detect the presence of active signal,

TABLE I
COMPARISON BETWEEN THE STANDARDIZED AND PROPOSED BOOTSTRAP IN TERMS OF SIGNALING DECODING (REQUIRED SNR)

Channel Types	SNR for Standardized Bootstrap	SNR for version signaling (Gain)		SNR for Proposed FD signaling (Gain)		SNR for Proposed TD signaling (Gain)	
		BW(4.5M)	BW(6M)	BW(4.5M)	BW(6M)	BW(4.5M)	BW(6M)
0dB Echo	**-11.8**	-15.7 (3.9)	-17.1	-14.6 (2.8)	-16.3 (4.5)	**-12.1 (0.3)**	-13.5 (1.7)
Mobile SFN	-9	-11.8 (2.8)	-13	**-9.8 (0.8)**	-10.9 (1.9)	**-9.8 (0.8)**	-10.9 (1.9)
TU6	-8.7	-11.4 (2.7)	-12.3	**-9 (0.3)**	-10.3 (1.6)	**-9 (0.3)**	-10.3 (1.6)

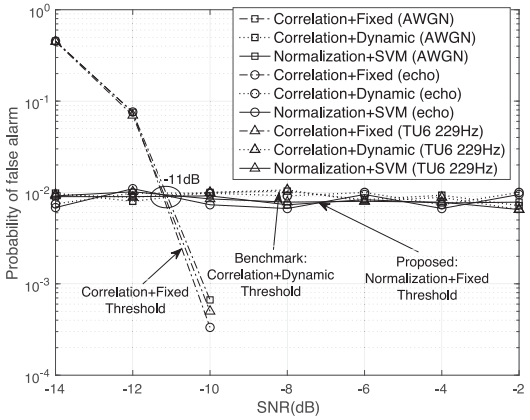

Fig. 12. Probability of false alarm by different schemes.

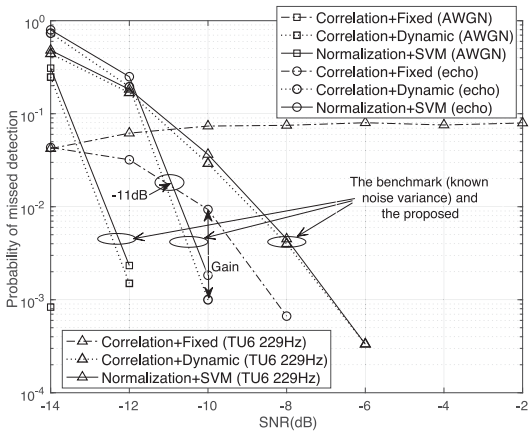

Fig. 13. Probability of missed detection by different schemes.

because the probability of reaching this threshold (i.e., probability of detection) is low. Referring to Fig. 13, P_{md} of the proposed scheme has a sharper decline than that of the static scheme in channels with SNR over -11dB. Assuming location1 and location2 with respective -11dB SNR and -10dB SNR, we can obtain a much lower P_{md} by utilizing the dynamic scheme and proposed scheme. Furthermore, the static correlation-based scheme does not work well in time-varying fast fading channel due to fluctuations of received signal power. Comparatively, the proposed scheme has almost the same performance with the dynamic scheme with known noise variance, which avoids the use of noise estimator and eliminates the impact of inaccurate noise estimation. Simulation results show that SVM is an efficient tool for derivation of the threshold under multiple channels with different noise powers, since only data close to the boundary contribute a lot to the model. Comparatively, the training data with good channel conditions are far from the boundary, which have little impact on this model. Note that the proposed synchronization and detection schemes can be directly applied to the standardized bootstrap because of the same TD structure. Further improvement on synchronization accuracy can be achieved based on our derivation like [25], [26], but it is beyond our scope.

B. Versioning and Signaling Decoding for Matched Receiver

This part will describe the performance evaluation of versioning and signaling decoding. Table I summarizes the decoding performances of the standardized and proposed bootstrap in terms of required SNR (in dB) with decoding SER equal to 10^{-2}. Fig. 14 to Fig. 16 compare the FD signaling error rate (SER) of the proposed bootstrap with the standardized bootstrap in typical use cases. The decoding performance of version signaling is also displayed here, as successful decoding of version information is prerequisite for subsequent operations. The matched versioning defined here indicates that the receiver has the same operating bandwidth with the transmitted signal, which is used to distinguish from the cross versioning latter. We can observe that the additional versioning has little impact on FD signaling decoding due to its maximum tolerance with only 1 bit capacity, but in return significant improvement can be achieved by exploiting more active subcarriers in all cases even when compatibility is taken into consideration. Over 1dB gain can be observed by DTTB network with 6MHz bandwidth, which is annotated as FD signaling (T = 1, R = 1). In addition, compared with the standardized bootstrap, the decoding performance of the proposed bootstrap for MCN with 4.5MHz bandwidth are about 2.8dB better than that of the standardized bootstrap in 0dB echo channel. Moreover, SER of the proposed scheme drops faster than the standardized one in mobile SFN and TU6 channels, and at least 0.3dB gain can be achieved by the proposed one. To sum up, the proposed bootstrap outperforms the standardized bootstrap in channels of strong multipath and fast time-variation even with the same bandwidth resources, which is consistent with the analysis in Section V-B. On this basis, over 1dB additional gain can be obtained by DTTB system with more bandwidth.

After we finish the decoding of FD signaling, the next step is to decode the additional TD signaling. Table I and Fig. 17 show the SER performance of TD signaling transmission. Incorrect decoded FD signaling will probably lead to false

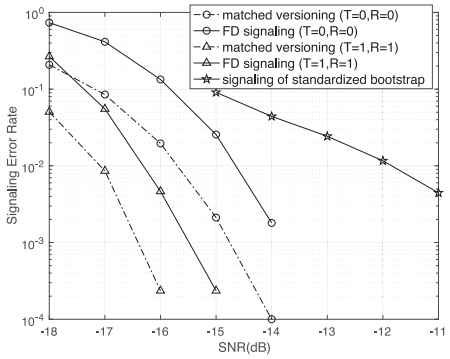

Fig. 14. FD SER performance comparison for matched receiver under 0db echo channel.

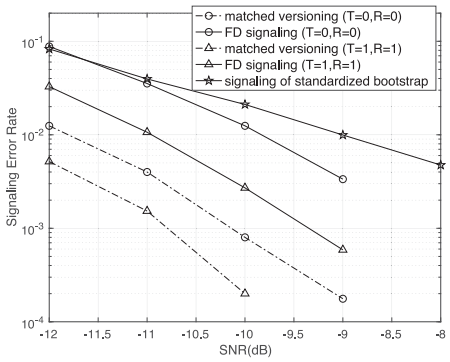

Fig. 15. FD SER performance comparison for matched receiver under Mobile SFN channel.

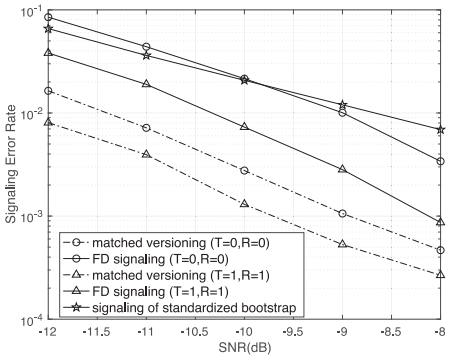

Fig. 16. FD SER performance comparison for matched receiver under TU6 channel.

decoding of TD signaling, so only 3 valid bits are transmitted in TD. A lower capacity in combination with Grey mapping provides larger tolerance to any distortion than the standardized bootstrap. From Table I, the required SNRs for TD signaling are indistinguishable from the FD signaling in Mobile SFN and TU6 channels since $P^{TD}(\overline{A}) \approx P(\overline{B})$ as analyzed in (70). However, significant sidelobes in echo channel will dominate the performance of TD signaling, because $P(B|\overline{A})$ is nonnegligible, which means $P^{TD}(\overline{A}) \approx P(B|\overline{A})P(\overline{A}) + P(\overline{B})$. In 0dB echo channel, $P(\overline{A})$ is the dominating factor because it has over 2.5dB higher required SNR than $P(\overline{B})$. In this case, $P(\overline{B}) \ll P(\overline{A})$, so $P^{TD}(\overline{A}) \approx P(B|\overline{A})P(\overline{A})$. It can be seen from Fig. 17 and Table I that at least 0.3dB better performance can be observed for the proposed 4.5MHz bootstrap in terms of

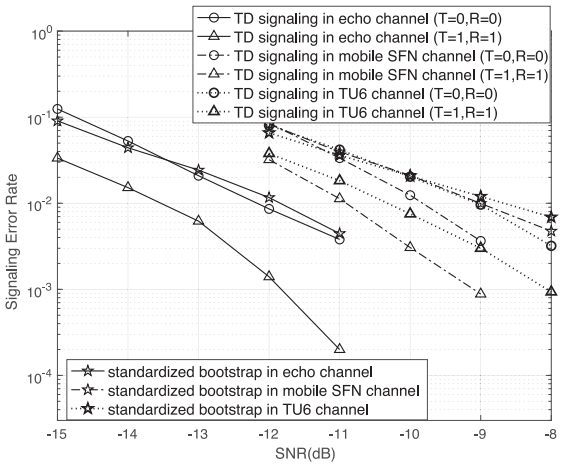

Fig. 17. TD SER performance comparison for matched receiver under multiple channels.

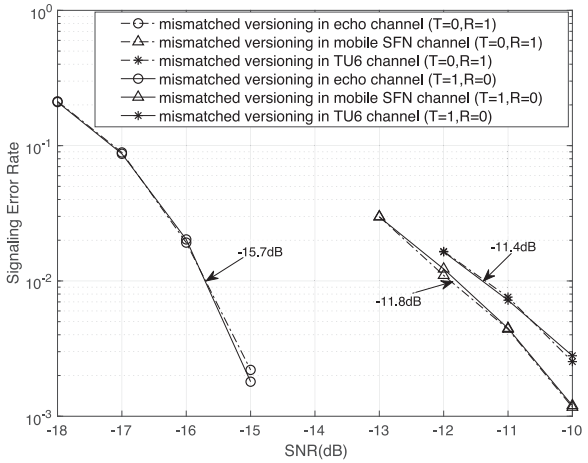

Fig. 18. Versioning performance for mismatched receiver under multiple channels.

required SNR. Furthermore, 6MHz system has over 1dB lower SNR than the 4.5Mhz system. Therefore, higher total capacity can be achieved by concurrent transmission in FD and TD without performance degradation.

C. Cross Versioning in Case of Mismatched Receiver

An adaptive bootstrap should allow cross versioning which means version information need to be decoded by mismatched receiver with different bandwidths. For instance, a MCN receiver is able to decode version signaling from 6MHz bootstrap in a 4.5MHz manner. If 6MHz bootstrap is received by a 4.5MHz receiver, the curves in Fig. 18 have a label of (T = 1, R = 0), and vice versa. The same performance can be observed comparing the two cases. From Table I and Fig. 18, we can see that cross versioning has the same performance with the matched versioning in the case of 4.5MHz operating bandwidth (T = 0, R = 0). The decoding performances of version signaling by mismatched receiver still have 3.9dB, 2.8dB and 2.7dB gain against the standardized bootstrap in 0dB echo, Mobile SFN and TU6 channels respectively. In this way, receiver is capable of blindly and stably identifying the

signal type from any transmission network, so that informed decision can be made sequentially.

VII. Conclusion

A novel bootstrap with adaptive bandwidth was proposed in this paper, which has significant improvement on the accuracy of signaling decoding by making the most of available bandwidth while maintaining the compatibility with MCN. The proposed bootstrap distinguishes the signaling by picking different modulating gold sequence in FD and applying cyclic shift in TD simultaneously, which has 3-bit higher signaling capacity than the standardized bootstrap. Version information indicating the occupied bandwidth can be decoded blindly by matched and mismatched receivers in severe scenario. Furthermore, improved receiver algorithms with regard to synchronization, spectrum sensing and signaling decoding are presented and validated accordingly. The proposed MNE scheme based on derived ML function outperforms the correlation based scheme in time-varying channels. In the case of unknown noise variance, the proposed combinative scheme of normalized energy estimator and SVM has a comparable performance on spectrum sensing with the ideal dynamic scheme, which requires perfect noise estimation. Compared with the TD signaling scheme of the standardized bootstrap, the proposed FD signaling scheme is more robust over 0dB echo, Mobile SFN and TU6 channels even if this bootstrap precedes a MCN signal with 4.5MHz bandwidth. In addition, over 1dB gain can be further achieved by exploiting more available bandwidth when this bootstrap precedes a DTTB signal. In this way, there is no need to call for a tradeoff between better performance and higher compatibility.

References

[1] R. W. Heath, N. González-Prelcic, S. Rangan, W. Roh, and A. M. Sayeed, "An overview of signal processing techniques for millimeter wave MIMO systems," *IEEE J. Sel. Topics Signal Process.*, vol. 10, no. 3, pp. 436–453, Apr. 2016.

[2] M. Shafi *et al.*, "5G: A tutorial overview of standards, trials, challenges, deployment, and practice," *IEEE J. Sel. Areas Commun.*, vol. 35, no. 6, pp. 1201–1221, Jun. 2017.

[3] D. Lecompte and F. Gabin, "Evolved multimedia broadcast/multicast service (eMBMS) in LTE-advanced: Overview and rel-11 enhancements," *IEEE Commun. Mag.*, vol. 50, no. 11, pp. 68–74, Nov. 2012.

[4] W. Zhang *et al.*, "Convergence of a terrestrial broadcast network and a mobile broadband network," *IEEE Commun. Mag.*, vol. 56, no. 3, pp. 74–81, Mar. 2018.

[5] D. Gomez-Barquero, D. Navratil, S. Appleby, and M. Stagg, "Point-to-multipoint communication enablers for the fifth generation of wireless systems," *IEEE Commun. Stand. Mag.*, vol. 2, no. 1, pp. 53–59, Mar. 2018.

[6] J. J. Gimenez, D. Gomez-Barquero, J. Morgade, and E. Stare, "Wideband broadcasting: A power-efficient approach to 5G broadcasting," *IEEE Commun. Mag.*, vol. 56, no. 3, pp. 119–125, Mar. 2018.

[7] J. Calabuig, J. F. Monserrat, and D. Gómez-Barquero, "5th generation mobile networks: A new opportunity for the convergence of mobile broadband and broadcast services," *IEEE Commun. Mag.*, vol. 53, no. 2, pp. 198–205, Feb. 2015.

[8] T. Stevens and S. Appleby, "Video delivery and challenges: Tv, broadcast and over the top," in *MediaSync*. Cham, Switzerland: Springer, 2018, pp. 547–564. [Online]. Available: https://link.springer.com/chapter/10.1007/978-3-319-65840-7_19#copyrightInformation

[9] D. He *et al.*, "System discovery and signaling transmission using bootstrap in ATSC 3.0," *IEEE Trans. Broadcast.*, vol. 62, no. 1, pp. 172–180, Mar. 2016.

[10] M. M. Wang, A. Agrawal, A. Khandekar, and S. Aedudodla, "Preamble design, system acquisition, and determination in modern OFDMA cellular communications: An overview," *IEEE Commun. Mag.*, vol. 49, no. 7, pp. 164–175, Jul. 2011.

[11] K. I. Pedersen, G. Berardinelli, F. Frederiksen, P. Mogensen, and A. Szufarska, "A flexible 5G frame structure design for frequency-division duplex cases," *IEEE Commun. Mag.*, vol. 54, no. 3, pp. 53–59, Mar. 2016.

[12] Y. Huang *et al.*, "Improved bootstrap design for frequency-domain signaling transmission," *IEEE Trans. Broadcast.*, vol. 63, no. 4, pp. 615–626, Dec. 2017.

[13] J. J. V. D. Beek, M. Sandell, and P. O. Borjesson, "ML estimation of time and frequency offset in OFDM systems," *IEEE Trans. Signal Process.*, vol. 45, no. 7, pp. 1800–1805, Jul. 1997.

[14] J. A. Zhang and X. Huang, "Autocorrelation based coarse timing with differential normalization," *IEEE Trans. Wireless Commun.*, vol. 11, no. 2, pp. 526–530, Feb. 2012.

[15] A. Mohebbi, H. Abdzadeh-Ziabari, and M. G. Shayesteh, "Novel coarse timing synchronization methods in OFDM systems using fourth-order statistics," *IEEE Trans. Veh. Technol.*, vol. 64, no. 5, pp. 1904–1917, May 2015.

[16] T. T. Nguyen *et al.*, "Robust spectrum sensing of DVB-T2 signal using the first preamble symbol," in *Proc. IEEE Int. Conf. Adv. Technol. Commun. (ATC)*, Ho Chi Minh City, Vietnam, Oct. 2013, pp. 261–265.

[17] M. Hamid, S. B. Slimane, W. V. Moer, and N. Bjorsell, "Spectrum sensing challenges: Blind sensing and sensing optimization," *IEEE Instrum. Meas. Mag.*, vol. 19, no. 2, pp. 44–52, Apr. 2016.

[18] B. Li, M. Sun, X. Li, A. Nallanathan, and C. Zhao, "Energy detection based spectrum sensing for cognitive radios over time-frequency doubly selective fading channels," *IEEE Trans. Signal Process.*, vol. 63, no. 2, pp. 402–417, Nov. 2015.

[19] G. Yang *et al.*, "Cooperative spectrum sensing in heterogeneous cognitive radio networks based on normalized energy detection," *IEEE Trans. Veh. Technol.*, vol. 65, no. 3, pp. 1452–1463, Mar. 2016.

[20] K. M. Thilina, K. W. Choi, N. Saquib, and E. Hossain, "Machine learning techniques for cooperative spectrum sensing in cognitive radio networks," *IEEE J. Sel. Areas Commun.*, vol. 31, no. 11, pp. 2209–2221, Nov. 2013.

[21] C.-C. Chang and C.-J. Lin, "LIBSVM: A library for support vector machines," *ACM Trans. Intell. Syst. Technol.*, vol. 2, no. 3, pp. 1–27, May 2011.

[22] L. Huang and C. C. Ko, "Performance of maximum-likelihood channel estimator for UWB communications," *IEEE Commun. Lett.*, vol. 8, no. 6, pp. 356–358, Jun. 2004.

[23] Y. Huang, D. He, Y. Zhao, Y. Xu, and W. Zhang, "A novel preamble design using LDM," in *Proc. IEEE Int. Symp. Broadband Multimedia Syst. Broadcast. (BMSB)*, Nara, Japan, Jun. 2016, pp. 1–5.

[24] P. Kryszkiewicz and H. Bogucka, "In-band-interference robust synchronization algorithm for an NC-OFDM system," *IEEE Trans. Commun.*, vol. 64, no. 5, pp. 2143–2154, May 2016.

[25] M. Rotoloni, S. Tomasin, and L. Vangelista, "Maximum likelihood estimation of time and carrier frequency offset for DVB-T2," *IEEE Trans. Broadcast.*, vol. 58, no. 1, pp. 77–86, Mar. 2012.

[26] X. Zhang, J. Liu, H. Li, and B. Himed, "Maximum likelihood synchronization for DVB-T2 in unknown fading channels," *IEEE Trans. Broadcast.*, vol. 61, no. 4, pp. 615–624, Dec. 2015.

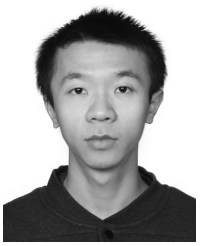

Yihang Huang received the bachelor's degree from the University of Electronic Science and Technology of China in 2014. He is currently pursuing the Ph.D. degree in information and communication engineering with Shanghai Jiao Tong University. His research interests include digital signal and related receiver algorithms design and key technologies for cooperation between DTTB and cellular systems.

Dazhi He received the Ph.D. degree in electronic engineering from Shanghai Jiao Tong University, Shanghai, China, in 2009, where he is currently an Associate Researcher with Cooperative Medianet Innovation Center. His research interests include wireless communications, smart transmission, and heterogeneous network.

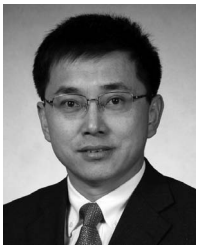

Wenjun Zhang received the B.S., M.S., and Ph.D. degrees in electronic engineering from Shanghai Jiao Tong University, Shanghai, China, in 1984, 1987, and 1989, respectively. After three years working as an Engineer with Philips, Nuremberg, Germany, he went back to his Alma Mater in 1993 and he has been a Full Professor with Shanghai Jiao Tong University since 1995. He was one of the main contributors of the Chinese DTTB Standard (DTMB) issued in 2006. He holds 142 patents and published 110 papers in international journals and conferences. He is the Chief Scientist of the Chinese Digital TV Engineering Research Centre (NERC-DTV), an industry/government consortium in DTV technology research and standardization, and the Director of Cooperative MediaNet Innovation Center, an excellence research cluster affirmed by the Chinese Government. His main research interests include video coding and wireless transmission, multimedia semantic analysis, and broadcast/broadband network convergence.

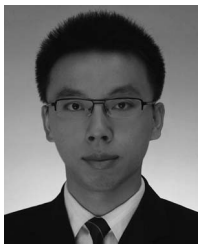

Yin Xu received the B.Sc. degree in information science and engineering from Southeast University, China, in 2009 and the master's and Ph.D. degrees in electronics engineering from Shanghai Jiao Tong University in 2011 and 2015, respectively, where he is currently an Assistant Professor. His main research interests include channel coding, advanced bit-interleaved coded modulation, and other physical layer technologies in broadcasting and 5G. He is quite active in participating in standardization progress in ATSC3.0 and 3GPP. He is highly interested in studying the theory and technology on converged broadcasting and broadband networks.

Yunfeng Guan received the Ph.D. degree from Zhejiang University in 2003. He is currently a Professor with Shanghai Jiao Tong University, a member of National Radio, Film and Television Standardization Technical Committee - subtechnical committee (SAC/TC239/SC2) of wireless transmission and coverage. He mainly engaged in the study of digital TV systems and wireless access systems. He is also one of the main drafters of the China Digital Terrestrial Television Transmission Standard GB20600-2006 (DTMB) and other important national DTV standards.